

Robot-DIFT: Distilling Diffusion Features for Geometrically Consistent Visuomotor Control

Yu Deng^{1*}, Yufeng Jin^{1*}, Xiaogang Jia²
 Jiahong Xue¹, Gerhard Neumann^{2,3}, Georgia Chalvatzaki^{1,4,5}
¹TU Darmstadt ²KIT ³FZI
⁴Hessian.AI ⁵Robotics Institute Germany *Equal contribution

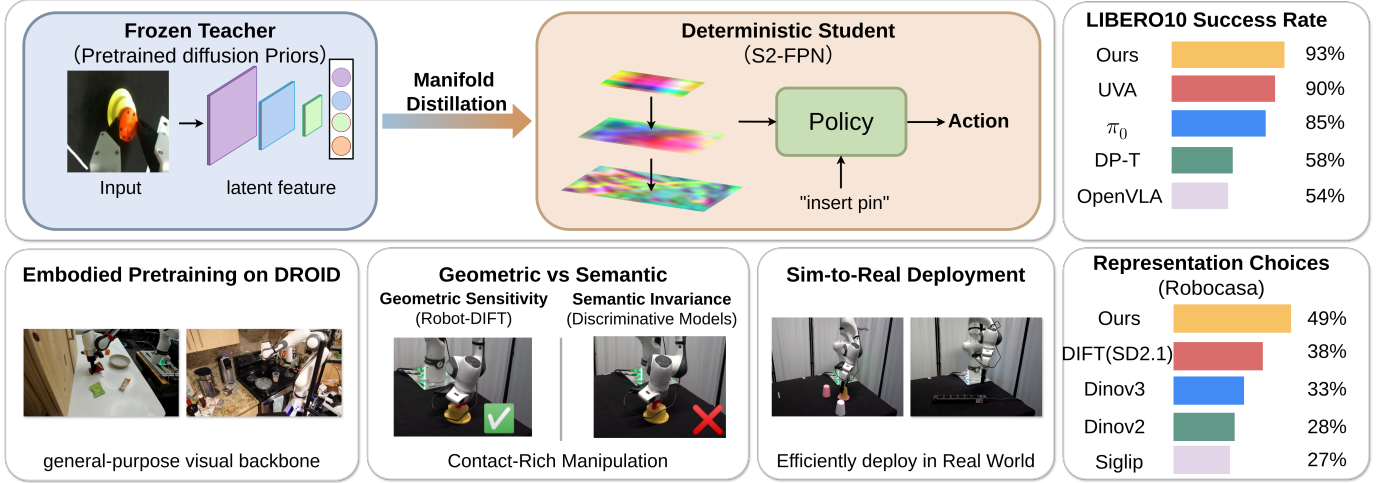


Fig. 1: **Robot-DIFT**: Bridging the Representation Mismatch for Contact-Rich Manipulation. **Geometric vs Semantic**: Unlike discriminative features that prioritize *semantic invariance*, Robot-DIFT preserves *spatial layout sensitivity* and *fine-grained detail* required to resolve surface normals and contact boundaries. **Manifold Distillation**: We distill the *pretrained generative manifold* into a deterministic *Spatial–Semantic Feature Pyramid Network (S2-FPN)* under a *frozen teacher constraint* to eliminate *stochasticity* and *latency*. **Embodied Pretraining**: We pretrain the backbone on *DROID* to align representations with the *geometric statistics* of manipulation environments for instruction-conditioned learning. **Experimental Validation**: Robot-DIFT overcomes the “blind spot” in fine-grained control, outperforming VLA on *LIBERO-10* and exceeds discriminative baselines in *Robocasa*.

Abstract—We hypothesize that a key bottleneck in generalizable robot manipulation is not solely data scale or policy capacity, but a structural mismatch between current visual backbones and the physical requirements of closed-loop control. While state-of-the-art vision encoders (including those used in VLAs) optimize for semantic invariance to stabilize classification, manipulation typically demands *geometric sensitivity*—the ability to map millimeter-level pose shifts to predictable feature changes. Their discriminative objective creates a “blind spot” for fine-grained control, whereas generative diffusion models inherently encode geometric dependencies within their latent manifolds, encouraging the preservation of dense multi-scale spatial structure. However, directly deploying stochastic diffusion features for control is hindered by stochastic instability, inference latency, and representation drift during fine-tuning. To bridge this gap, we propose *Robot-DIFT*, a framework that decouples the source of geometric information from the process of inference via Manifold Distillation. By distilling a frozen diffusion teacher into a deterministic Spatial-Semantic Feature Pyramid Network (S2-FPN), we retain the rich geometric priors of the generative model while ensuring temporal stability, real-time execution, and robustness against drift. Pretrained on the large-scale *DROID* dataset, *Robot-DIFT* demonstrates superior geometric consistency and control performance compared to

leading discriminative baselines, supporting the view that *how a model learns to see* dictates how well it can learn to act.

I. INTRODUCTION

We often observe a characteristic failure mode in contact-rich manipulation: a policy can reach the right object, yet still oscillates at the final millimeters—missing a peg-in-hole, slipping during insertion, or repeatedly “tapping” the surface without committing to stable contact [12, 44]. Such behaviors suggest that the controller is not lacking capacity, but is operating on visual features that do not change reliably with small pose perturbations. In other words, the policy may perceive *what* to interact with, yet lacks a representation that varies *predictably* with *where and how* to establish contact.

A key bottleneck that hinders generalization in robot manipulation is often not the policy architecture or data scale alone, but a *representation mismatch* between widely used visual backbones and the physical requirements of closed-loop control. While pretrained encoders like DINOV2 [31] and SigLIP [46] offer rich semantic priors, they are optimized for

image-level invariance rather than the fine-grained spatial correspondence required for precision tasks. Consequently, these representations often collapse subtle geometric nuances—such as surface normals and contact boundaries—that are critical for reactive control. This leaves the policy *visually aware* of the object but *physically blind* to the precise geometry of contact.

In contrast, contact-rich manipulation demands *geometric sensitivity*, where millimeter-level shifts in object pose map to distinct, predictable changes in the feature space. While recognition-oriented objectives explicitly suppress such local variations to aid recognition, diffusion features (DIFT) [47] preserve them. DIFT exhibits strong *spatial layout* sensitivity—even in texture-poor regions—providing the dense geometric fidelity required to bridge the gap between semantic perception and actuation.

Alternatively, methods leveraging point-cloud representations [15, 45] provide explicit 3D geometry, but they introduce practical and statistical trade-offs: they typically require accurate camera robot calibration and depth alignment, and their effective spatial resolution can be limited by sensor noise and network capacity, yielding sparse or incomplete geometric cues. Moreover, point-cloud data are often less standardized across sensors and scenes and are typically less abundant than RGB, making it harder to scale training and compare methods consistently.

Whether leveraging robotics-specific pretraining (e.g., R3M [29], VIP [26]) or adapting generalist vision foundation models (e.g., SigLIP [46], DINOv2 [31]) within Vision-Language-Action (VLA) frameworks (e.g., OpenVLA [18]), state-of-the-art approaches largely rely on objectives that emphasize *semantic separability* rather than *geometric reconstruction*. Consequently, these representations exhibit a “blind spot” in fine-grained control: they can robustly identify *what* an object is, yet often fail to resolve *where* it is with the precision needed for insertion or grasping [16, 27]. Crucially, this limitation stems from a fundamental *representation mismatch* induced by discriminative training objectives, which cannot be trivially resolved by simply scaling data or policy capacity.

Conversely, generative diffusion models offer representations with rich multi-scale structure that retain both high-level semantics and fine spatial detail. However, directly utilizing diffusion inference for online control faces three practical challenges: (1) *Stochasticity*: the iterative denoising process introduces sampling noise that can translate into action jitter; (2) *Latency*: multi-step diffusion inference is computationally prohibitive for high-frequency closed-loop execution; and (3) *Representation Drift*: naively fine-tuning the backbone with policy gradients can distort the pretrained generative manifold, leading to the collapse of the very geometric priors required for robust interaction.

To bridge this gap, we propose **Robot-DIFT**, a framework that distills the rich geometric priors of diffusion models into a deterministic backbone for control. Our key insight is to decouple the *source* of geometric information (pretrained diffusion priors) from the *process* of real-time inference. Instead of running the heavy, stochastic diffusion process

online, we distill the pretrained generative manifold into a deterministic *Spatial–Semantic Feature Pyramid Network (S2-FPN)* via a student–teacher approach, which we term *Manifold Distillation*: a training-only procedure that transfers diffusion’s geometric priors into a stable student representation under a frozen teacher constraint. This distillation process uses the frozen teacher as a geometric anchor, preserving the dense, geometry-preserving structure of the diffusion model while enforcing the temporal stability and inference speed required for closed-loop robotics. Concretely, Robot-DIFT addresses these challenges by (i) replacing stochastic diffusion inference with a single deterministic Student forward pass to reduce jitter, (ii) introducing a multi-level *S2-FPN* to retain semantics and fine geometry across scales, and (iii) constraining adaptation with a frozen Teacher anchor to mitigate drift. To encourage broad task and embodiment coverage, we pretrain this backbone on *DROID*, a large-scale robot demonstration dataset [17], and leverage available task descriptors (and language when present) for instruction-conditioned learning.

Our contributions are:

- We identify a critical *representation mismatch* in robotic perception: semantic-invariant discriminative often suppress the geometric sensitivity required for high-precision, contact-rich control.
- We propose *Manifold Distillation* with a *Spatial–Semantic Feature Pyramid Network (S2-FPN)*, a unified framework that distills diffusion priors into a multi-scale, fully deterministic backbone suitable for real-time execution.
- We provide a general-purpose visual backbone pretrained on *DROID* that effectively bridges pixel-level spatial fidelity with high-level semantic grounding for instruction-following tasks.
- We demonstrate that Robot-DIFT significantly improves *geometric sensitivity* and control performance over strong discriminative baselines, validating that preserving spatial gradients is essential for precise actuation.

II. RELATED WORK

A. Visual Representations for Visuomotor Policy Learning

Early work in imitation learning (IL) and reinforcement learning (RL) typically trained shallow convolutional networks or ResNet-based encoders from scratch on task-specific data, achieving strong performance in constrained environments but limited robustness to visual distractors, or novel objects [5, 14, 28, 32, 34, 35]. To improve sample efficiency and generalization, subsequent approaches adopted pre-trained visual representations. Self-supervised objectives such as masked reconstruction (e.g., MVP) and contrastive learning in egocentric or manipulation-centric datasets have demonstrated improved robustness over learning from scratch [23, 28, 29, 43]. However, these representations often require domain-specific pre-training or fine-tuning and do not naturally scale to the visual diversity captured by internet-scale data. More importantly, their training objectives emphasize invariance rather than the geometric precision required for contact-rich manipulation.

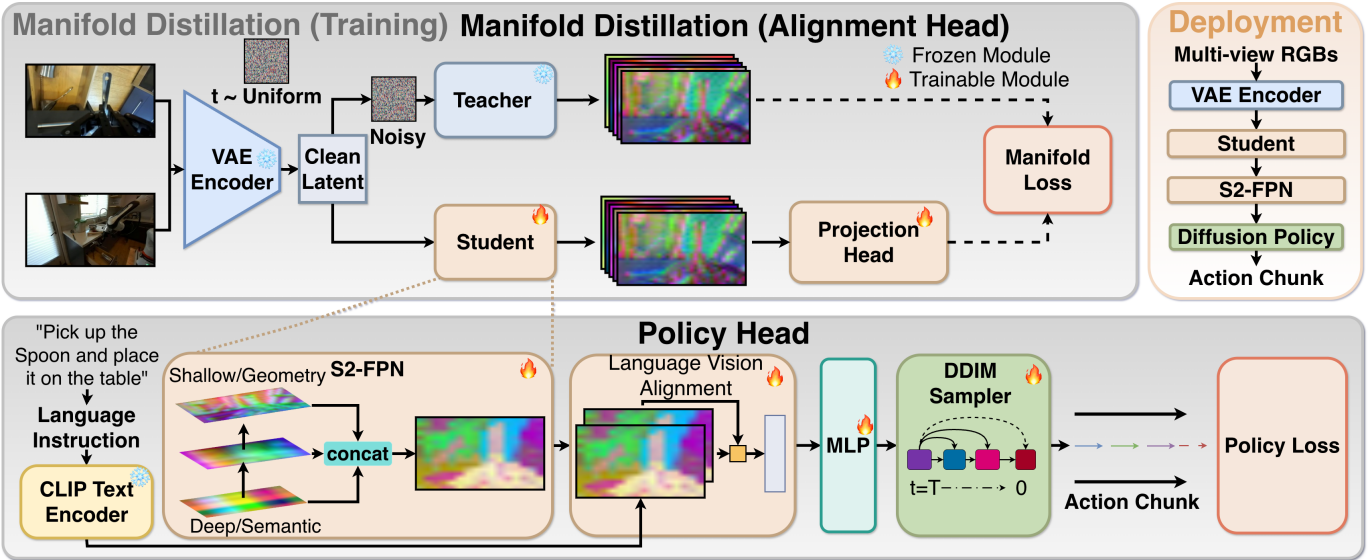


Fig. 2: **Overview of Robot-DIFT.** Our framework distills generative diffusion priors into a deterministic backbone for efficient robotic control. **Manifold Distillation:** A Student U-Net is trained to replicate the multi-scale feature manifold of a frozen Teacher. The S2-FPN fuses these features to capture semantic context and fine geometry, while a Manifold Loss anchors the Student to the diffusion prior to prevent representation drift. **Deployment:** By discarding the Teacher, we enable a single-forward-pass pipeline that preserves geometric sensitivity without the latency or stochasticity of iterative sampling.

B. Foundation Visual Models and Vision-Language–Action Policies

Recent progress has been driven by foundation visual models integrated into Vision Language Action (VLA) [1, 2, 13, 19, 22, 36]. Pretrained encoders such as CLIP [33], SigLIP [46], and DINOv2 [31] are widely used as frozen backbones in generalist policies, enabling semantic grounding and instruction following [18, 42]. Similarly, RT-1 and RDT-1B rely on pretrained discriminative encoders (e.g., EfficientNet or SigLIP) to process visual observations [3, 24]. While highly effective at recognizing *what* an object is, these representations prioritize semantic invariance, which is structurally misaligned with manipulation tasks that require millimeter-level geometric accuracy. Empirical studies show that such representations often lack the dense spatial fidelity needed for precise contact and pose reasoning [29]. Attempts to compensate via explicit depth fusion or point-cloud backbones improve geometry but introduce additional computational overhead and sensor dependence [7, 9, 15].

C. Generative Diffusion Models for Perception and Control

Generative diffusion models provide a fundamentally different representational bias [6, 37, 39]. Trained via iterative denoising, diffusion models are forced to preserve fine-grained spatial structure, and recent analyses reveal that their U-Net activations encode dense pixel-level correspondences and hierarchical part–whole relationships [40, 47]. Methods such as DIFT and CleanDIFT demonstrate that diffusion features extracted from clean images retain both semantic context and geometric detail, outperforming discriminative features on correspondence tasks. In robotics, however, diffusion models have primarily been applied to model the *action* distribution, as

in Diffusion Policy and RDT-1B, while perception continues to rely on standard discriminative encoders [5, 24]. Directly using diffusion features for control is nontrivial: their dependence on stochastic noise and timesteps induces temporal instability, and naïve fine-tuning on limited robot data risks representation drift that degrades pretrained geometric priors.

Overall, existing approaches either employ discriminative visual backbones with strong policies or adopt generative models exclusively in the action space while leaving perception invariant-focused. This leaves a gap between semantic generalization and geometric precision at the level of the visual representation. Robot-DIFT addresses this gap by introducing a generative *visual* backbone for real-time control. Through deterministic distillation of pretrained diffusion representations into a noise-free Spatial–Semantic Feature Pyramid Network, Robot-DIFT preserves diffusion’s dense geometric priors while ensuring stability and efficiency for closed-loop manipulation.

III. METHOD

We propose Robot-DIFT, a framework that distills the geometric priors of a generative diffusion model into a deterministic visual backbone for robotic control (see Fig. 2). Our approach consists of two phases: *Manifold Distillation (Training)*. In *Manifold Distillation* (Sec. III-C) we train a Student U-Net on clean latents to match the multi-scale, noise-conditioned feature manifold of a frozen diffusion Teacher. To retain both semantic context and fine geometry, the Student is augmented with a *Spatial–Semantic Feature Pyramid Network (S2-FPN)* (Sec. III-B) that fuses decoder features across resolutions. A training-only alignment loss anchors all Student decoder layers to the Teacher manifold, mitigating

representation drift while remaining compatible with policy learning. *Deterministic Inference (Deployment)*. At deployment, we discard the Teacher and alignment heads, retaining only the distilled Student and policy. This yields a single forward-pass visual backbone that preserves diffusion-based geometric sensitivity without the latency or stochasticity of iterative diffusion inference.

A. Preliminaries

We build upon Latent Diffusion Models (LDMs) [37], specifically Stable Diffusion v2.1. Unlike standard diffusion models [6, 11] that operate in pixel space, LDMs utilize a pretrained Variational Autoencoder (VAE) [20] to map an RGB image $\mathbf{x} \in \mathbb{R}^{H \times W \times 3}$ into a compressed latent representation $\mathbf{z}_0 = \mathcal{E}(\mathbf{x}) \in \mathbb{R}^{h \times w \times c}$. This compression enables high-resolution synthesis while maintaining computational efficiency.

During pretraining, a forward diffusion process gradually injects Gaussian noise into the latent \mathbf{z}_0 according to a fixed variance schedule. At an arbitrary timestep t , the noisy latent \mathbf{z}_t can be sampled in closed form via:

$$\mathbf{z}_t = \sqrt{\bar{\alpha}_t} \mathbf{z}_0 + \sqrt{1 - \bar{\alpha}_t} \boldsymbol{\epsilon}, \quad \boldsymbol{\epsilon} \sim \mathcal{N}(\mathbf{0}, \mathbf{I}), \quad (1)$$

where $\bar{\alpha}_t$ is the noise schedule coefficient. A time-conditional U-Net $\epsilon_\theta(\mathbf{z}_t, t, \mathbf{c})$ is then trained to denoise \mathbf{z}_t by minimizing the objective $\mathbb{E}[\|\boldsymbol{\epsilon} - \epsilon_\theta(\mathbf{z}_t, t, \mathbf{c})\|_2^2]$, conditioned on context \mathbf{c} (e.g., text instructions).

Crucially for our approach, we exploit the *internal representations* of the U-Net rather than its final generative output. The U-Net features a hierarchical encoder-decoder architecture with skip connections. Recent findings, DIFT [47] demonstrates that the intermediate feature maps within the U-Net decoder encode dense, pixel-level semantic and geometric correspondences that are robust to nuisance variations. In this work, we treat the pretrained SD2.1 U-Net as a frozen “Teacher,” leveraging its multi-scale decoder features (specifically under noise-conditioned inputs \mathbf{z}_t) to supervise the training of our deterministic “Student” backbone. A more comprehensive discussion of the diffusion manifold and the U-Net decoder’s multi-scale hierarchy is provided in Appendix ??.

B. Student Architecture: S2-FPN

To achieve deterministic and real-time control, our Student network processes clean latents \mathbf{z}_0 via a single forward pass, avoiding the computational cost and stochastic variance of iterative denoising. To capture both *what* to manipulate (semantics) and *where* to interact (geometry), we adopt a *Spatial-Semantic Feature Pyramid Network (S2-FPN)* that fuses multi-scale diffusion features.

a) *Multi-Scale Feature Extraction*.: Given an image x , we extract three feature maps from the Student U-Net decoder:

$$\mathcal{S} = \{\mathbf{s}^{(k)}\}_{k=1}^3 = \{\mathbf{s}^{(us3)}, \mathbf{s}^{(us6)}, \mathbf{s}^{(us8)}\}, \quad (2)$$

ordered from coarse to fine resolution. These scales are selected to jointly capture global semantic context and fine-grained geometric detail across resolutions. This choice is em-

pirically validated, and we analyze alternative layer selections in the ablation study (Sec. IV-C).

We select these levels to span the semantic-geometric trade-off: the coarse feature $\mathbf{s}^{(us3)}$ provides global context, the mid-level $\mathbf{s}^{(us6)}$ captures affordance structure, and the high-resolution $\mathbf{s}^{(us8)}$ preserves local edges critical for precise contact.

b) *Global-to-Fine Feature Fusion*.: Since direct concatenation is brittle due to scale and semantic mismatches, we propose the Global-to-Fine Fusion module to progressively inject global semantic context into high-resolution geometric maps (Fig. 2). Let $\mathbf{s}^{(i)}$ denote the raw feature at pyramid level i (with $i \in \{1, 2, 3\}$ corresponding to $\{\mathbf{s}^{(us3)}, \mathbf{s}^{(us6)}, \mathbf{s}^{(us8)}\}$, ordered from coarse to fine resolution) and $\mathbf{M}^{(i)}$ the fused map. We initialize the pyramid with $\mathbf{M}^{(1)} = \mathbf{s}^{(1)}$, corresponding to the coarsest semantic feature. We recursively compute:

$$\mathbf{M}^{(i)} = \text{ConvBlock}\left(\mathbf{s}^{(i)} \oplus \text{Upsample}\left(\mathbf{M}^{(i-1)}\right)\right), \quad (3)$$

where \oplus is channel-wise concatenation and ConvBlock is a residual stack of convolution, group normalization, and GELU, where Upsample(\cdot) uses bilinear interpolation to resize the coarser feature map to match the spatial resolution of $\mathbf{s}^{(i)}$ (so that element-wise fusion is well-defined). This yields spatially aligned maps that preserve fine geometry while being informed by global semantics. The S2-FPN mirrors the spatial resolutions and channel structure of the Stable Diffusion U-Net decoder, enabling layer-wise alignment and simplifying Manifold Distillation. By explicitly propagating global semantics into fine-resolution features, S2-FPN enhances geometric sensitivity without sacrificing semantic coherence.

c) *Language-vision alignment*.: The visual feature map $\mathbf{M}_v \in \mathbb{R}^{B \times C_v \times H \times W}$ must be converted into a fixed-dimensional representation for the policy without discarding spatial structure. Unlike prior designs that fuse language and vision by a simple token concatenation, we explicitly align language and visual tokens via cross-attention. We first flatten the map into a sequence of HW visual tokens, $\mathbf{X}_v \in \mathbb{R}^{B \times HW \times C_v}$, and apply 2D RoPE positional encoding to preserve spatial coordinates [10, 41]. In parallel, we obtain *frozen* language tokens $\mathbf{X}_\ell \in \mathbb{R}^{B \times N_\ell \times C_\ell}$ from a CLIP text encoder. To enable cross-modal interaction under a shared embedding size, we project both modalities to the same dimension C using lightweight adapters: $\hat{\mathbf{X}}_v = \psi_v(\text{LN}(\mathbf{X}_v)) \in \mathbb{R}^{B \times HW \times C}$ and $\hat{\mathbf{X}}_\ell = \psi_\ell(\text{LN}(\mathbf{X}_\ell)) \in \mathbb{R}^{B \times N_\ell \times C}$. We then perform multi-head cross-attention with language tokens as queries and visual tokens as keys/values:

$$\begin{aligned} \tilde{\mathbf{H}}^{(m)} &= \text{MHA}\left(\text{query} = \hat{\mathbf{X}}_\ell, \text{key} = \hat{\mathbf{X}}_v^{(m)}, \text{value} = \hat{\mathbf{X}}_v^{(m)}\right) \\ &\in \mathbb{R}^{B \times N_\ell \times C}, \end{aligned} \quad (4)$$

where m indexes the input image/view (for a single image, set $m=1$). Intuitively, using language tokens as queries focuses computation on the instruction-relevant subspace, substantially reducing complexity compared to attending over all visual tokens as queries while still exploiting dense visual keys/values.

For multi-image inputs, we leverage GPU parallelism by computing $\tilde{\mathbf{H}}^{(m)}$ independently for each image/view and then aggregating across views via element-wise max pooling:

$$\tilde{\mathbf{H}} = \max_{m \in \{1, \dots, M\}} \tilde{\mathbf{H}}^{(m)} \in \mathbb{R}^{B \times N_\ell \times C}. \quad (5)$$

We feed $\tilde{\mathbf{H}}$ through a standard Transformer block. The output is a fixed set of N_ℓ cross-attended tokens $\mathbf{H} \in \mathbb{R}^{B \times N_\ell \times C}$. Finally, we flatten \mathbf{H} and apply a small MLP to obtain the final observation embedding consumed by the policy.

C. Manifold Distillation

To enable robust transfer of the encoder across tasks and environments while preserving fine-grained spatial cues and mitigating representation drift, we employ *Manifold Distillation*.

We instantiate a frozen Teacher U-Net f_{θ_0} from the pre-trained model (SD2.1) and create a Student f_θ with an identical U-Net backbone. The Student’s U-Net parameters are initialized by weight copying ($\theta \leftarrow \theta_0$), while the additional S2-FPN modules are randomly initialized. During training, only the Student is updated while the Teacher remains fixed.

The Student operates on clean latents z_0 , whereas the Teacher naturally defines a noise-conditioned diffusion manifold through noisy latents z_τ at timestep τ , where SD2.1 uses 1000 diffusion steps ($\tau \in \{0, \dots, 999\}$). To bridge this domain gap, we align the Student’s clean features to the Teacher’s noise-conditioned features. Specifically, for each training sample, we draw τ uniformly from $[0, 999]$, enforcing consistency across the full noise spectrum. This compels the Student to hallucinate the geometric priors present at various noise levels while maintaining deterministic inputs for control.

Crucially, we perform alignment over all decoder blocks. At a sampled timestep τ , we record the activation from every Teacher decoder block and denote it as $\mathbf{f}_\tau^{(k)}$, where $k \in \{1, \dots, K\}$ indexes all decoder blocks. We map the Student’s features $\mathbf{s}^{(k)}$ into the Teacher’s embedding space using lightweight, timestep-conditioned projection heads $\{g_\phi^{(k)}\}_{k=1}^K$. Note that the Teacher features serve as the ground-truth anchor and are not projected. Gradients are stopped on the Teacher branch, so the alignment loss constrains only the Student to stay close to the pretrained diffusion manifold, preventing drift induced by policy-only fine-tuning.

We ℓ_2 -normalize the feature vectors for stability:

$$\mathbf{u}_\tau^{(k)} = \frac{g_\phi^{(k)}(\mathbf{s}^{(k)}, \tau)}{\|g_\phi^{(k)}(\mathbf{s}^{(k)}, \tau)\|_2}, \quad \mathbf{v}_\tau^{(k)} = \frac{\mathbf{f}_\tau^{(k)}}{\|\mathbf{f}_\tau^{(k)}\|_2}, \quad (6)$$

where $\mathbf{s}^{(k)}$ are Student features and $\mathbf{f}_\tau^{(k)}$ are the frozen Teacher features. The alignment loss minimizes the negative cosine similarity:

$$\mathcal{L}_{\text{align}} = \mathbb{E}_{(x, s, a) \sim \mathcal{D}, \tau \sim \mathcal{T}} \left[\sum_{k=1}^K w_k \left(1 - \langle \mathbf{u}_\tau^{(k)}, \mathbf{v}_\tau^{(k)} \rangle \right) \right]. \quad (7)$$

where \mathcal{D} denotes the training dataset and we use uniform weights ($w_k=1$) for all blocks. Overall, we optimize a joint

objective that combines the policy loss with manifold alignment:

$$\mathcal{L} = \mathcal{L}_{\text{policy}} + \lambda \mathcal{L}_{\text{align}}. \quad (8)$$

We anneal the alignment weight $\lambda(t)$ to allow initial adaptation before relaxing constraints:

$$\lambda(t) = \lambda_{\min} + (\lambda_0 - \lambda_{\min}) \cdot \max \left(0, 1 - \frac{t}{T_{\text{decay}}} \right). \quad (9)$$

where t denotes the training step, $\lambda_0=0.1$ and $\lambda_{\min}=0.001$ balance the alignment and policy losses for stable optimization, and we set $T_{\text{decay}} = \lfloor 0.5 T \rfloor$ following common schedule choices [25]. At deployment, we discard the Teacher U-Net and all alignment heads, retaining only the clean Student model for deterministic control. For more details regarding the optimization protocol and specific training hyperparameters, see Appendix ??.

IV. EXPERIMENTS

In this section, we comprehensively evaluate Robot-DIFT to validate its efficacy in learning geometry-aware representations for robotic manipulation. Our experimental design aims to answer three primary research questions:

- **Q1 (Representation Choice):** To what extent do distilled diffusion priors outperform standard self-supervised baselines (e.g., *CLIP*, *DINOv2*) in contact-rich and geometry-sensitive manipulation tasks?
- **Q2 (System Efficiency):** How does the proposed method compare against *vision-language-action* (VLA) and *video action models* in terms of the accuracy-latency trade-off?
- **Q3 (Real-World Applicability):** To what degree can the learned representations generalize to physical robot setups for solving coarse-to-fine manipulation challenges?

To address **Q1**, we benchmark on *RoboCasa* [30] (Sec. IV-A). For **Q2**, we compare against representative VLA and video-action models on *LIBERO-10* (Sec. IV-B). We also validate our specific design choices (multi-scale fusion and annealing) via ablation studies in Sec. IV-C. Finally, answering **Q3**, we deploy Robot-DIFT on a physical Franka Emika Panda robot to demonstrate real-world generalization (Sec. IV-D).

A. Representation Choice

We evaluate Robot-DIFT on *RoboCasa* to isolate how the *visual representation* impacts contact-rich, geometry-sensitive manipulation.

a) Benchmark.: *RoboCasa* [30] is a large-scale simulation framework covering diverse everyday manipulation tasks with extensive intra-task variations in scenes, object instances, and initial robot/object states. Such variation induces different geometric constraints even within the same task (e.g., surrounding clutter can invalidate certain grasp approaches), requiring strong generalization and making *RoboCasa* a challenging testbed for representation robustness. We evaluate the *RoboCasa* tasks listed in Table I, which cover diverse everyday manipulation skills with frequent contact and tight spatial constraints (e.g., articulated interactions such as doors/drawers,

toggle-like state changes, and precise button/press or placement behaviors). Each task provides 50 human demonstrations. For training, we train each model for 200 epochs, and for evaluation we rollout 50 episodes per task.

b) Baselines and Protocol.: To isolate representation effects from policy and optimization choices, all methods use Diffusion Policy [5] and identical training recipe under an encoder-swap protocol; only the **frozen** visual encoder is varied. Observations consist of RGB images resized to 256×256 (with language instructions when available). We compare against *CLIP* [33] (vision–language pretraining with semantically aligned image features), *SigLIP* [46] (sigmoid-contrastive vision–language pretraining), *DINOv2* [31] (self-supervised visual features for transfer), and *DINOv3* [38] (a scaled DINO-family self-supervised backbone with improved transfer). We further include *DIFT (SD2.1)* as a diffusion-feature baseline, obtained via manifold distillation from a Stable Diffusion teacher [37] and using the resulting deterministic Student to extract *clean* features at inference time. Robot-DIFT (Ours) distills the same diffusion priors but performs manifold distillation on the robotics dataset *DROID* [17], producing a robot-adapted diffusion-feature backbone. Complete implementation details, including training schedules and evaluation hyperparameters, are provided in Appendix ??.

c) Results and Analysis.: Table I shows that diffusion-based representations consistently outperform standard vision backbones in contact-rich manipulation. Specifically, *DIFT (SD2.1)* achieves a mean success rate of 0.38, surpassing non-diffusion baselines such as *CLIP* and *DINOv3* (mean 0.27). Our proposed **Robot-DIFT** further increases this margin to 0.49 (+0.11), attaining the highest success rate on **18/24** tasks. The performance gains are most pronounced in tasks requiring precise contact and spatial reasoning under clutter, notably *OpenDoubleDoor* (+0.74), *CoffeeServeMug* (+0.44), and *CoffeePressButton* (+0.30).

These results support the hypothesis that diffusion features preserve richer spatial structures compared to semantically-invariant discriminative features. While contrastive or self-distillation objectives often sacrifice fine-grained detail for semantic category-level invariance, the convolutional U-Net and synthesis-based objective in Stable Diffusion inherently capture spatial coherence and global-local layouts. By fine-tuning these priors on robotics-specific data (*DROID*), Robot-DIFT effectively aligns with the geometric statistics of complex manipulation environments.

B. Comparison with VLA and Video Action Models

While large *vision–language–action* (VLA) and video models excel at semantic grounding and long-horizon reasoning, their massive scale often makes fine-tuning and deployment on robot-specific data computationally prohibitive [18, 21]. In this section, we assess whether Robot-DIFT can serve as a parameter-efficient alternative. Using the *LIBERO-10* benchmark, we compare downstream manipulation performance against practical deployment metrics, including inference latency and model capacity. These results, summarized in

Table II, highlight the trade-offs between representation power and operational efficiency.

a) Benchmark and protocol.: We adopt the *LIBERO-10* dataset and protocol from [21]: each task is evaluated in 50 environments with different seeds, and we report the average success rate across all 10 tasks (full settings in Appendix ??). For inference-time measurement, we report the runtime of a single action-trajectory: all methods except *OpenVLA* infer a 16-step sequence (8 executed steps), while *OpenVLA* predicts one action per forward pass and is executed 8 times to match the control horizon [18, 21].

b) Baselines.: We include representative *action-only*, *VLA*, and *video-action* baselines. *DP-C* and *DP-T* are *Diffusion Policy* variants [5]. *OpenVLA* is a large-scale VLA finetuned for manipulation [18]. *UniPi* is a video-based policy [8]. π_0 and π_0 -*FAST* are open-source VLA flow models [2]. Finally, *UVA* (*Unified Video Action*) jointly models video and action with decoupled diffusion heads [21]. Robot-DIFT (Ours) performs manifold distillation on *DROID* [17] to obtain a deterministic backbone, then trains a standard *Diffusion Policy* head on *LIBERO-10* while keeping the visual backbone frozen.

c) Results and Analysis.: Table II summarizes the results. Robot-DIFT achieves the best overall success rate (**0.93**) while being the most efficient method (**0.01s** per trajectory). Compared to the strongest baseline *UVA* [21], Robot-DIFT improves success by +0.03 and reduces inference time by $23 \times$ (0.01 s vs. 0.23 s). It also outperforms π_0 [2] in success (0.93 vs. 0.85) while being 9× faster (0.01 s vs. 0.09 s). In contrast, large VLA approaches are slower and less effective: *OpenVLA* [18] reaches 0.54 success at 1.52 s, and *UniPi* [8] fails to solve the tasks (0.00) with high latency (24.07 s). Overall, these results indicate that Robot-DIFT provides a superior accuracy–latency trade-off for language-conditioned manipulation on *LIBERO-10*.

C. Ablation Study

We conduct ablations to validate the two key design choices in Sec. III: (i) multi-scale feature extraction at deployment after distillation, and (ii) alignment-weight annealing during distillation. All experiments are evaluated on a geometry-sensitive RoboCasa subset with *Pressing Buttons* and *Insertion* tasks, which require precise contact and tight spatial tolerances.

a) Multi-Scale Feature Extraction.: We first complete Manifold Distillation to obtain a deterministic Student backbone, freeze it, and train an identical downstream policy across all variants. We compare single-scale decoder features against our multi-scale design. *SingleScale-us3/us6/us8* uses a single Student decoder feature map $\mathbf{s}^{(us3)}$, $\mathbf{s}^{(us6)}$, or $\mathbf{s}^{(us8)}$, while *MultiScale (Ours)* fuses $\{\mathbf{s}^{(us3)}, \mathbf{s}^{(us6)}, \mathbf{s}^{(us8)}\}$ via S2-FPN global-to-fine aggregation. This ablation isolates whether combining coarse semantic context with fine-grained geometry yields more reliable contact-aware control than any single resolution.

Category	Task	CLIP [33]	SigLIP [46]	DINOv2 [31]	DINOv3 [38]	DIFT (SD2.1)	Robot-DIFT (Ours)
Pick and Place	PnPCabToCounter	0.10	0.02	0.10	0.02	0.06	0.10
	PnPCounterToCab	0.00	0.00	0.00	0.00	0.04	0.08
	PnPCounterToMicrowave	0.02	0.02	0.02	0.02	0.06	0.10
	PnPCounterToSink	0.00	0.00	0.00	0.00	0.08	0.06
	PnPCounterToStove	0.06	0.06	0.06	0.06	0.04	0.08
	PnPMicrowaveToCounter	0.00	0.02	0.00	0.04	0.08	0.08
	PnPSinkToCounter	0.04	0.06	0.04	0.08	0.10	0.26
	PnPStoveToCounter	0.00	0.00	0.00	0.02	0.04	0.20
Doors	OpenSingleDoor	0.14	0.30	0.34	0.44	0.56	0.58
	OpenDoubleDoor	0.00	0.10	0.04	0.04	0.18	0.92
	CloseDoubleDoor	0.08	0.58	0.62	0.54	0.60	0.60
	CloseSingleDoor	0.70	0.70	0.80	0.78	0.62	0.84
Drawers	OpenDrawer	0.20	0.44	0.38	0.56	0.70	0.60
	CloseDrawer	0.82	0.78	0.94	1.00	1.00	1.00
Twisting Knobs	TurnOnStove	0.24	0.26	0.30	0.42	0.58	0.44
	TurnOffStove	0.12	0.08	0.12	0.24	0.22	0.22
Turning Levers	TurnOnSinkFaucet	0.24	0.40	0.42	0.36	0.56	0.62
	TurnOffSinkFaucet	0.50	0.62	0.60	0.78	0.78	0.74
	TurnSinkSpout	0.32	0.44	0.32	0.40	0.40	0.48
Pressing Buttons	CoffeePressButton	0.22	0.46	0.44	0.68	0.70	1.00
	TurnOnMicrowave	0.22	0.44	0.46	0.64	0.66	0.82
	TurnOffMicrowave	0.42	0.52	0.54	0.52	0.72	0.90
Insertion	CoffeeServeMug	0.10	0.08	0.14	0.32	0.30	0.74
	CoffeeSetupMug	0.02	0.04	0.02	0.02	0.10	0.18
Avg. Task Success Rate		0.19	0.27	0.28	0.33	0.38	0.49

TABLE I: **RoboCasa benchmark comparison.** We report the success rate (%) on the validation set over 50 rollouts per task. The best score per task is in **bold**.

Method	Success Rate \uparrow	Speed (s) \downarrow
DP-C [5]	0.53	0.50
DP-T [5]	0.58	0.36
OpenVLA [18]	0.54	1.52
UniPi [8]	0.00	24.07
π_0 [2]	0.85	0.09
π_0 -FAST [2]	0.60	0.09
UVA [21]	0.90	0.23
Robot-DIFT (Ours)	0.93	0.01

TABLE II: **LIBERO-10 benchmark.** Comparison of average success rates and inference speed. Robot-DIFT (Ours) distills diffusion priors via manifold distillation on *DROID* [17] and trains a standard Diffusion Policy [5] on LIBERO-10 with a *frozen* backbone. All methods, except OpenVLA, infer 16 action steps per trajectory with 8 executed steps. OpenVLA infers one action at a time, so it is run 8 times to match the inference time for 8 executed actions.

Single-scale variants expose the trade-off between global context and local geometry: coarse features retain task-level semantics but under-resolve contact details, whereas fine features preserve edges but are less robust to global distractors.

Variant	Pressing Buttons	Insertion
<i>Feature Extraction</i>		
SingleScale-us3	0.39	0.13
SingleScale-us6	0.52	0.28
SingleScale-us8	0.46	0.24
MultiScale (Ours)	0.90	0.46
<i>Alignment Schedule</i>		
NoAnneal	0.76	0.31
Anneal (Ours)	0.90	0.46

TABLE III: **Ablation study on RoboCasa.** We report success rates (%) on contact-rich tasks. MultiScale features and Annealing strategies significantly improve geometric precision.

By fusing across scales, MultiScale (Ours) aims to provide both signals. As shown in Table III, MultiScale achieves the highest mean success (0.68), outperforming the best single-scale variant by +0.28. Notably, it improves success to 0.90 on *Pressing Buttons* (vs. 0.39–0.52) and to 0.46 on *Insertion* (vs. 0.28), demonstrating that coarse-to-fine fusion is critical for precise alignment under clutter and occlusion.

b) Alignment-Weight Annealing.: We evaluate the annealing strategy for the distillation weight $\lambda(t)$ in Eq. (7). *NoAnneal* keeps $\lambda(t) = \lambda_0$ throughout training, enforcing

a constant constraint to the Teacher manifold, while *Anneal (Ours)* linearly decays $\lambda(t)$ from λ_0 to λ_{\min} over T_{decay} steps. This comparison tests whether a time-varying constraint better balances manifold preservation and task adaptation.

Anneal (Ours) consistently outperforms *NoAnneal*, increasing mean success from 0.54 to 0.68 (+0.15), with gains on both *Pressing Buttons* ($0.76 \rightarrow 0.90$) and *Insertion* ($0.31 \rightarrow 0.46$). These results indicate that strong early alignment anchors the student to the diffusion geometry, while gradual relaxation enables specialization to task-specific contact dynamics; in contrast, a constant constraint over-restricts adaptation and degrades performance.

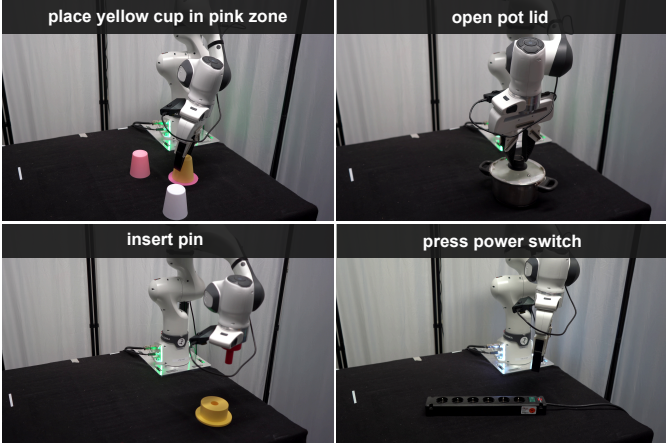


Fig. 3: Real-robot task suite. We evaluate four manipulation tasks that progressively increase *geometric sensitivity*, from coarse semantic grounding to contact-rich interaction with tight tolerances: *Sort Cup* (place yellow cup in pink zone), *Open Lid*, *Insert Pin*, and *Press Switch*.

D. Real-Robot Experiments

To validate our hypothesis that geometric sensitivity is the key bottleneck in contact-rich manipulation, we evaluate Robot-DIFT on a set of real-robot tasks that explicitly disentangle semantic recognition from spatial precision. The tasks are designed to progressively increase geometric sensitivity—from coarse, semantics-driven objectives to contact-rich interactions with tight tolerances—so that failures can be attributed to insufficient spatial precision rather than category recognition. All experiments are conducted on a 7-DoF Franka Emika Panda robot equipped with two ZED cameras: a wrist-mounted camera for hand–eye coordination and a third-person camera observing the workspace. Object poses and target placements are reset at the beginning of each trial to ensure experimental rigor.

a) *Tasks.*: We evaluate four tasks spanning increasing levels of geometric precision: (1) *Sort Cup*: placing a yellow cup into a pink target zone among multiple cups, primarily testing semantic grounding. (2) *Open Lid*: opening a pot lid, requiring stable contact and continuous pose regulation. (3) *Insert Pin*: a high-precision insertion task with approximately 2 mm clearance, where small spatial errors directly cause failure. (4) *Press Switch*: toggling a power switch with a small

effective contact region ($< 4 \text{ cm}^2$), making success sensitive to local geometry and precise end-effector placement.

b) *Baselines and Implementation Details.*: To ensure a rigorous comparison of visual representations, we standardize the policy architecture across all experiments using the Diffusion Policy implementation from *DROID* [17]. We evaluate our method against two state-of-the-art semantic baselines: *DINOv2* [31] and *SigLIP* [46]. For all runs, the visual backbone is kept **frozen** to explicitly isolate the quality of pre-trained features. We train the policy head for 10K gradient steps on identical datasets containing limited demonstrations per task: *Sort Cup* (36), *Open Lid* (31), *Insert Pin* (35), and *Press Button* (35). During deployment, we employ a receding horizon control scheme with action chunking [48]: predicting a 16-step sequence and executing the first 8 steps closed-loop. Further hyperparameters and training details are detailed in the Appendix ??.

Visual Backbone	Sort	Open	Insert	Press	Avg.
DINOv2 [31]	0.55	0.60	0.05	0.35	0.39
SigLIP [46]	0.40	0.45	0.0	0.10	0.24
Robot-DIFT (Ours)	0.50	0.55	0.35	0.55	0.49

TABLE IV: Performance comparison under normal lighting conditions.

c) *Results and Analysis.*: We report the task success rate averaged over 20 trials per task (Table IV). Robot-DIFT (Ours) achieves the highest average success rate of **0.49**, surpassing *DINOv2* (0.39) and *SigLIP* (0.24). A detailed breakdown reveals a significant performance dichotomy based on task precision. On coarse manipulation tasks relying on semantic understanding (*Sort Cup*, *Open Lid*), *DINOv2* remains competitive, slightly outperforming our method (e.g., 0.60 vs. 0.55 on *Open Lid*). This confirms that high-level semantic features are sufficient for gross motion planning.

However, Robot-DIFT demonstrates a decisive advantage in geometry-sensitive, high-precision tasks. For *Insert Pin*—which requires sub-centimeter alignment—our method improves success rates from 0.05 (*DINOv2*) to **0.35**. Similarly, on *Press Switch*, we observe a +0.20 improvement over the strongest baseline. These results suggest that while standard ViT baselines excel at semantic categorization, they often lack the fine-grained spatial granularity required for tight-tolerance manipulation. In contrast, Robot-DIFT effectively distills spatial cues critical for precise contact and alignment.

V. CONCLUSION

Robot-DIFT demonstrates that diffusion-based intermediate representations capture geometric nuances often absent in discriminative backbones, particularly for contact-rich manipulation. Through manifold distillation, we extract these spatial priors into a deterministic framework, bypassing the latency and stochasticity of iterative sampling to enable real-time control. While effective for the rigid-body tasks evaluated here, the generalization of these features to non-rigid objects—such

as ropes or cloth—and tasks requiring long-horizon temporal reasoning warrants further investigation. Furthermore, our study is limited to Stable Diffusion v2.1 [37]; distilling from recent video generative models [4] represents a promising path toward incorporating richer spatiotemporal priors. Future work will explore adaptive mechanisms to dynamically weight semantic and geometric cues, prioritizing global context during task planning and local precision during physical interaction.

REFERENCES

- [1] Johan Bjorck, Fernando Castañeda, Nikita Cherniadev, Xingye Da, Runyu Ding, Linxi Fan, Yu Fang, Dieter Fox, Fengyuan Hu, Spencer Huang, et al. Gr00t n1: An open foundation model for generalist humanoid robots. *arXiv preprint arXiv:2503.14734*, 2025.
- [2] Kevin Black, Noah Brown, Danny Driess, Adnan Es-mail, Michael Equi, Chelsea Finn, Niccolò Fusai, Lachy Groom, Karol Hausman, Brian Ichter, et al. π_0 : A vision-language-action flow model for general robot control. *corr, abs/2410.24164*, 2024. doi: 10.48550. *arXiv preprint ARXIV.2410.24164*.
- [3] Anthony Brohan, Noah Brown, Justice Carbajal, Yevgen Chebotar, Joseph Dabis, Chelsea Finn, Keerthana Gopalakrishnan, Karol Hausman, Alex Herzog, Jasmine Hsu, et al. Rt-1: Robotics transformer for real-world control at scale. *arXiv preprint arXiv:2212.06817*, 2022.
- [4] Tim Brooks, Bill Peebles, Connor Holmes, Will DePue, Yufei Guo, Li Jing, David Schnurr, Joe Taylor, Troy Luhman, Eric Luhman, et al. Video generation models as world simulators. *OpenAI Blog*, 1(8):1, 2024.
- [5] Cheng Chi, Zhenjia Xu, Siyuan Feng, Eric Cousineau, Yilun Du, Benjamin Burchfiel, Russ Tedrake, and Shuran Song. Diffusion policy: Visuomotor policy learning via action diffusion. *The International Journal of Robotics Research*, 44(10-11):1684–1704, 2025.
- [6] Prafulla Dhariwal and Alexander Nichol. Diffusion models beat gans on image synthesis. *Advances in neural information processing systems*, 34:8780–8794, 2021.
- [7] Atalay Donat, Xiaogang Jia, Xi Huang, Aleksandar Taranovic, Denis Blessing, Ge Li, Hongyi Zhou, Hanyi Zhang, Rudolf Lioutikov, and Gerhard Neumann. Towards fusing point cloud and visual representations for imitation learning. *arXiv preprint arXiv:2502.12320*, 2025.
- [8] Yilun Du, Sherry Yang, Bo Dai, Hanjun Dai, Ofir Nachum, Josh Tenenbaum, Dale Schuurmans, and Pieter Abbeel. Learning universal policies via text-guided video generation. *Advances in neural information processing systems*, 36:9156–9172, 2023.
- [9] Siddhant Haldar and Lerrel Pinto. Point policy: Unifying observations and actions with key points for robot manipulation. *arXiv preprint arXiv:2502.20391*, 2025.
- [10] Byeongho Heo, Song Park, Dongyoon Han, and Sangdoo Yun. Rotary position embedding for vision transformer. In *European Conference on Computer Vision*, pages 289–305. Springer, 2024.
- [11] Jonathan Ho, Ajay Jain, and Pieter Abbeel. Denoising diffusion probabilistic models. *Advances in neural information processing systems*, 33:6840–6851, 2020.
- [12] Sigmund H Høeg, Yilun Du, and Olav Egeland. Streaming diffusion policy: Fast policy synthesis with variable noise diffusion models. *arXiv preprint arXiv:2406.04806*, 2024.
- [13] Physical Intelligence, Kevin Black, Noah Brown, James Darpinian, Karan Dhabalia, Danny Driess, Adnan Es-mail, Michael Equi, Chelsea Finn, Niccolò Fusai, Manuel Y. Galliker, Dibya Ghosh, Lachy Groom, Karol Hausman, Brian Ichter, Szymon Jakubczak, Tim Jones, Liyiming Ke, Devin LeBlanc, Sergey Levine, Adrian Li-Bell, Mohith Mothukuri, Suraj Nair, Karl Pertsch, Allen Z. Ren, Lucy Xiaoyang Shi, Laura Smith, Jost Tobias Springenberg, Kyle Stachowicz, James Tanner, Quan Vuong, Homer Walke, Anna Walling, Haohuan Wang, Lili Yu, and Ury Zhilinsky. $\pi_{0.5}$: a vision-language-action model with open-world generalization, 2025. URL <https://arxiv.org/abs/2504.16054>.
- [14] Xiaogang Jia, Qian Wang, Atalay Donat, Bowen Xing, Ge Li, Hongyi Zhou, Onur Celik, Denis Blessing, Rudolf Lioutikov, and Gerhard Neumann. Mail: Improving imitation learning with selective state space models. In *8th Annual Conference on Robot Learning*, 2024.
- [15] Xiaogang Jia, Qian Wang, Anrui Wang, Han A Wang, Balázs Gyenes, Emiliyan Gospodinov, Xinkai Jiang, Ge Li, Hongyi Zhou, Weiran Liao, et al. Pointmappolicy: Structured point cloud processing for multi-modal imitation learning. *arXiv preprint arXiv:2510.20406*, 2025.
- [16] Siddharth Karamcheti, Suraj Nair, Annie S Chen, Thomas Kollar, Chelsea Finn, Dorsa Sadigh, and Percy Liang. Language-driven representation learning for robotics. *arXiv preprint arXiv:2302.12766*, 2023.
- [17] Alexander Khazatsky, Karl Pertsch, Suraj Nair, Ashwin Balakrishna, Sudeep Dasari, Siddharth Karamcheti, Soroush Nasiriany, Mohan Kumar Srirama, Lawrence Yunliang Chen, Kirsty Ellis, et al. Droid: A large-scale in-the-wild robot manipulation dataset. In *Robotics: Science and Systems*, 2024.
- [18] Moo Jin Kim, Karl Pertsch, Siddharth Karamcheti, Ted Xiao, Ashwin Balakrishna, Suraj Nair, Rafael Rafailov, Ethan Foster, Grace Lam, Pannag Sanketi, et al. Openvla: An open-source vision-language-action model. *arXiv preprint arXiv:2406.09246*, 2024.
- [19] Moo Jin Kim, Chelsea Finn, and Percy Liang. Fine-tuning vision-language-action models: Optimizing speed and success. *arXiv preprint arXiv:2502.19645*, 2025.
- [20] Diederik P Kingma and Max Welling. Auto-encoding variational bayes. *arXiv preprint arXiv:1312.6114*, 2013.
- [21] Shuang Li, Yihuai Gao, Dorsa Sadigh, and Shuran Song. Unified video action model. *arXiv preprint arXiv:2503.00200*, 2025.
- [22] Xinghang Li, Peiyan Li, Minghuan Liu, Dong Wang, Jirong Liu, Bingyi Kang, Xiao Ma, Tao Kong, Hanbo Zhang, and Huaping Liu. Towards generalist robot

policies: What matters in building vision-language-action models. *arXiv preprint arXiv:2412.14058*, 2024.

[23] Kevin Qinghong Lin, Jinpeng Wang, Mattia Soldan, Michael Wray, Rui Yan, Eric Z Xu, Difei Gao, Rong-Cheng Tu, Wenzhe Zhao, Weijie Kong, et al. Egocentric video-language pretraining. *Advances in Neural Information Processing Systems*, 35:7575–7586, 2022.

[24] Songming Liu, Lingxuan Wu, Bangguo Li, Hengkai Tan, Huayu Chen, Zhengyi Wang, Ke Xu, Hang Su, and Jun Zhu. Rdt-1b: a diffusion foundation model for bimanual manipulation. *arXiv preprint arXiv:2410.07864*, 2024.

[25] Ilya Loshchilov and Frank Hutter. Sgdr: Stochastic gradient descent with warm restarts. *arXiv preprint arXiv:1608.03983*, 2016.

[26] Yecheng Jason Ma, Shagun Sodhani, Dinesh Jayaraman, Osbert Bastani, Vikash Kumar, and Amy Zhang. Vip: Towards universal visual reward and representation via value-implicit pre-training. *arXiv preprint arXiv:2210.00030*, 2022.

[27] Arjun Majumdar, Karmesh Yadav, Sergio Arnaud, Jason Ma, Claire Chen, Sneha Silwal, Aryan Jain, Vincent-Pierre Berges, Tingfan Wu, Jay Vakil, et al. Where are we in the search for an artificial visual cortex for embodied intelligence? *Advances in Neural Information Processing Systems*, 36:655–677, 2023.

[28] Ajay Mandlekar, Danfei Xu, Josiah Wong, Soroush Nasiriany, Chen Wang, Rohun Kulkarni, Li Fei-Fei, Silvio Savarese, Yuke Zhu, and Roberto Martín-Martín. What matters in learning from offline human demonstrations for robot manipulation. In *Conference on Robot Learning*, pages 1678–1690. PMLR, 2022.

[29] Suraj Nair, Aravind Rajeswaran, Vikash Kumar, Chelsea Finn, and Abhinav Gupta. R3m: A universal visual representation for robot manipulation. *arXiv preprint arXiv:2203.12601*, 2022.

[30] Soroush Nasiriany, Abhiram Maddukuri, Lance Zhang, Adeet Parikh, Aaron Lo, Abhishek Joshi, Ajay Mandlekar, and Yuke Zhu. Robocasa: Large-scale simulation of everyday tasks for generalist robots. *arXiv preprint arXiv:2406.02523*, 2024.

[31] Maxime Oquab, Timothée Darcet, Théo Moutakanni, Huy Vo, Marc Szafraniec, Vasil Khalidov, Pierre Fernandez, Daniel Haziza, Francisco Massa, Alaaeldin El-Nouby, et al. Dinov2: Learning robust visual features without supervision. *arXiv preprint arXiv:2304.07193*, 2023.

[32] Simone Parisi, Aravind Rajeswaran, Senthil Purushwalkam, and Abhinav Gupta. The unsurprising effectiveness of pre-trained vision models for control. In *international conference on machine learning*, pages 17359–17371. PMLR, 2022.

[33] Alec Radford, Jong Wook Kim, Chris Hallacy, Aditya Ramesh, Gabriel Goh, Sandhini Agarwal, Girish Sastry, Amanda Askell, Pamela Mishkin, Jack Clark, et al. Learning transferable visual models from natural language supervision. In *International conference on ma-* chine learning, pages 8748–8763. PMLR, 2021.

[34] Moritz Reuss, Maximilian Li, Xiaogang Jia, and Rudolf Lioutikov. Goal-conditioned imitation learning using score-based diffusion policies. In *Robotics: Science and Systems*, 2023.

[35] Moritz Reuss, Ömer Erdinç Yağmurlu, Fabian Wenzel, and Rudolf Lioutikov. Multimodal diffusion transformer: Learning versatile behavior from multimodal goals. *arXiv preprint arXiv:2407.05996*, 2024.

[36] Moritz Reuss, Hongyi Zhou, Marcel Rühle, Ömer Erdinç Yağmurlu, Fabian Otto, and Rudolf Lioutikov. Flower: Democratizing generalist robot policies with efficient vision-language-action flow policies. *arXiv preprint arXiv:2509.04996*, 2025.

[37] Robin Rombach, Andreas Blattmann, Dominik Lorenz, Patrick Esser, and Björn Ommer. High-resolution image synthesis with latent diffusion models. In *Proceedings of the IEEE/CVF conference on computer vision and pattern recognition*, pages 10684–10695, 2022.

[38] Oriane Siméoni, Huy V Vo, Maximilian Seitzer, Federico Baldassarre, Maxime Oquab, Cijo Jose, Vasil Khalidov, Marc Szafraniec, Seungeun Yi, Michaël Ramamonjisoa, et al. Dinov3. *arXiv preprint arXiv:2508.10104*, 2025.

[39] Yang Song, Jascha Sohl-Dickstein, Diederik P Kingma, Abhishek Kumar, Stefano Ermon, and Ben Poole. Score-based generative modeling through stochastic differential equations. *arXiv preprint arXiv:2011.13456*, 2020.

[40] Nick Stracke, Stefan Andreas Baumann, Kolja Bauer, Frank Fundel, and Björn Ommer. Cleandift: Diffusion features without noise. In *Proceedings of the Computer Vision and Pattern Recognition Conference*, pages 117–127, 2025.

[41] Jianlin Su, Murtadha Ahmed, Yu Lu, Shengfeng Pan, Wen Bo, and Yunfeng Liu. Roformer: Enhanced transformer with rotary position embedding. *Neurocomputing*, 568:127063, 2024.

[42] Octo Model Team, Dibya Ghosh, Homer Walke, Karl Pertsch, Kevin Black, Oier Mees, Sudeep Dasari, Joey Hejna, Tobias Kreiman, Charles Xu, et al. Octo: An open-source generalist robot policy. *arXiv preprint arXiv:2405.12213*, 2024.

[43] Tete Xiao, Ilija Radosavovic, Trevor Darrell, and Jitendra Malik. Masked visual pre-training for motor control. *arXiv preprint arXiv:2203.06173*, 2022.

[44] Han Xue, Jieji Ren, Wendi Chen, Gu Zhang, Yuan Fang, Guoying Gu, Huazhe Xu, and Cewu Lu. Reactive diffusion policy: Slow-fast visual-tactile policy learning for contact-rich manipulation. In *Proceedings of Robotics: Science and Systems (RSS)*, 2025.

[45] Yanjie Ze, Gu Zhang, Kangning Zhang, Chenyuan Hu, Muhan Wang, and Huazhe Xu. 3d diffusion policy: Generalizable visuomotor policy learning via simple 3d representations. *arXiv preprint arXiv:2403.03954*, 2024.

[46] Xiaohua Zhai, Basil Mustafa, Alexander Kolesnikov, and Lucas Beyer. Sigmoid loss for language image pre-training. In *Proceedings of the IEEE/CVF international*

conference on computer vision, pages 11975–11986, 2023.

- [47] Junyi Zhang, Charles Herrmann, Junhwa Hur, Luisa Polania Cabrera, Varun Jampani, Deqing Sun, and Ming-Hsuan Yang. A tale of two features: Stable diffusion complements dino for zero-shot semantic correspondence. *Advances in Neural Information Processing Systems*, 36:45533–45547, 2023.
- [48] Tony Z Zhao, Vikash Kumar, Sergey Levine, and Chelsea Finn. Learning fine-grained bimanual manipulation with low-cost hardware. *arXiv preprint arXiv:2304.13705*, 2023.